J. Fluid Mech. (2008), *vol.* 599, *pp.* 111–120.
doi:10.1017/S0022112008000177 Printed in the United Kingdom

Spatially distributed control for optimal drag reduction of the flow past a circular cylinder

PHILIPPE PONCET[1,2], ROLAND HILDEBRAND[3], GEORGES-HENRI COTTET[3] AND PETROS KOUMOUTSAKOS[4]

[1]Université de Toulouse, INSA, GMM 135 avenue de Rangueil, F-31077 Toulouse, France
[2]CNRS, Institut de Mathématiques de Toulouse, Equipe MIP, F-31077 Toulouse, France
[3]Laboratoire Jean Kuntzmann, CNRS and Université de Grenoble, BP 53, F-38041 Grenoble, France
[4]Computational Science, ETH Zurich, CH-8092, Switzerland

(Received 5 June 2007 and in revised form 17 December 2007)

We report high drag reduction in direct numerical simulations of controlled flows past circular cylinders at Reynolds numbers of 300 and 1000. The flow is controlled by the azimuthal component of the tangential velocity of the cylinder surface. Starting from a spanwise-uniform velocity profile that leads to high drag reduction, the optimization procedure identifies, for the same energy input, spanwise-varying velocity profiles that lead to higher drag reduction. The three-dimensional variations of the velocity field, corresponding to modes A and B of three-dimensional wake instabilities, are largely responsible for this drag reduction. The spanwise wall velocity variations introduce streamwise vortex braids in the wake that are responsible for reducing the drag induced by the primary spanwise vortices shed by the cylinder. The results demonstrate that extending two-dimensional controllers to three-dimensional flows is not optimal as three-dimensional control strategies can lead efficiently to higher drag reduction.

1. Introduction

What is the maximum drag reduction that can be achieved in bluff body flows for a given energy of the controller? Are two-dimensional control strategies sufficient for drag reduction in three-dimensional flows? We address these questions via direct numerical simulations (DNS) of flows past circular cylinders controlled by spatial variations of the azimuthal component of the wall velocity.

Circular cylinders are widely considered as prototypical configurations for the study of bluff body flows. Drag-inducing mechanisms of cylinder flows involve a nonlinear interaction between the vortical structures in the wake and the generation of vorticity on the cylinder surface. The three-dimensional instabilities of the wake (Barkley & Henderson 1996; Williamson 1996) are related to mechanisms of drag production, while modifications of the cylinder shape and its velocity can be optimized in order to reduce the drag of the flow (Choi, Jeon & Kim 2008).

In this work we are interested in drag reduction induced by modifications of the tangential component of the wall velocity. A uniform, albeit unsteady, velocity on the cylinder surface has been shown to induce very high drag reduction in experiments (Tokumaru & Dimotakis 1991) and simulations (Dennis, Nguyen & Kocabiyik 2000; Poncet 2004) of cylinders undergoing rotary oscillations. Additional controllers can be devised by modifying the wall velocity profile (Kim & Choi 2005;

Milano & Koumoutsakos 2002). In Milano & Koumoutsakos (2002) two-dimensional simulations were performed for flows past a circular cylinder controlled by azimuthal variations of the tangential wall velocity. The optimal velocity profile was obtained using an evolutionary optimization procedure leading to high drag reduction. This velocity profile was then extended uniformly in the spanwise direction leading to drag reduction for three-dimensional flows (Poncet, Cottet & Koumoutsakos 2005; Poncet 2005). Hence one may conjecture that two-dimensional control strategies obtained from relevant experiments and simulations would provide an efficient method of identifying optimal wall velocity profiles that can then be extended to the control of three-dimensional flows. Open issues include the robustness of the velocity profiles with respect to three-dimensional perturbations as well as the extent to which the efficiency of two-dimensional control strategies could be improved using three-dimensional wall velocity profiles. There is mounting evidence (Lim & Lee 2004; Kim & Choi 2005; Dobre, Hangan & Vickery 2006) that three-dimensional controllers may lead to enhanced drag reduction that is beyond what is possible by two-dimensional controllers. This evidence complements the fact that, in uncontrolled flows, three-dimensional instabilities in the cylinder wake are associated with drag levels which are below those of the base two-dimensional flows.

In this paper we consider a systematic development of three-dimensional control strategies for cylinder flows by varying the distributions of the azimuthal component of the velocity on the cylinder surface. We start from an optimal spanwise-uniform profile that has been obtained for two-dimensional cylinder wakes in Milano & Koumoutsakos (2002). We then consider, for a given control energy, parametric modulations of this profile along the spanwise direction. We identify, using a simple design of experiments approach (Box & Wilson 1951), optimal parameters that result in spanwise velocity variations leading to drag reduction that is over four times more efficient than the initial two-dimensional control strategy. Though flow control using spanwise variations of the wall velocity has been presented Kim & Choi (2005), the control parameters in the present work differ in two respects. First, we consider tangential velocities instead of blowing–suction. Second, Kim & Choi (2005) considered large wavelengths for the modulation of the cylinder. We use harmonic variations, instead of subharmonics, of the cylinder span as for a given energy level this choice produces higher levels of axial vorticity. The production of axial vorticity near the cylinder surface plays an important role in drag reduction as is discussed in the next section.

2. Incompressible flows past circular cylinders

We consider the three-dimensional flow of an incompressible viscous fluid past a circular cylinder at Reynolds numbers ($Re = U_\infty D/\nu$) of 300 and 1000, where U_∞, ν denote respectively the free-stream velocity and the viscosity of the fluid and $D = 2R$ denotes the diameter of the cylinder. A representative view of the cylinder wake structures as obtained in experiments (Williamson 1996) and in DNS (Poncet 2004) is depicted in figure 1.

2.1. *Governing equations and numerical methods*

We consider the incompressible Navier–Stokes equations in their vorticity–velocity ($\boldsymbol{\omega}$–$\boldsymbol{u}$) formulation:

$$\frac{\partial \boldsymbol{\omega}}{\partial t} + \boldsymbol{u}\cdot\nabla\boldsymbol{\omega} = \boldsymbol{\omega}\cdot\nabla\boldsymbol{u} + \nu\Delta\boldsymbol{\omega} \tag{2.1}$$

with $\boldsymbol{\omega} = \nabla\times\boldsymbol{u}$ and $\nabla\cdot\boldsymbol{u} = 0$. These equations are complemented with the no-slip boundary condition on the moving surface of the cylinder. Using a cylindrical

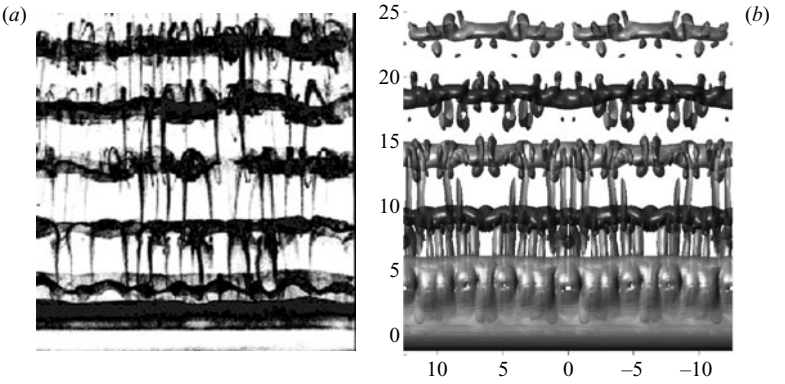

FIGURE 1. Wake representations of the flow past a circular cylinder at $Re = 300$ as depicted by dye visualizations in experiments Williamson (1996) (*a*), and by vorticity isosurfaces in DNS Poncet (2004) (*b*).

coordinate system $(\boldsymbol{e}_r, \boldsymbol{e}_\theta, \boldsymbol{e}_z)$ these boundary conditions are expressed as

$$\boldsymbol{u}_{r=R} = U_r(\theta, z, t)\boldsymbol{e}_r + U_\theta(\theta, z, t)\,\boldsymbol{e}_\theta + U_z(\theta, z, t)\boldsymbol{e}_z. \tag{2.2}$$

In the present simulations the spanwise and normal wall velocity components are set to zero. The flow is controlled by varying the steady azimuthal component of the wall velocity ($U_\theta(\theta, z)$). Throughout this paper we consider a cylinder of radius 1. The computational box is the cylindrical domain $1 \leqslant r \leqslant R_{\max}$, $0 \leqslant \theta \leqslant 2\pi$, $-L/2 \leqslant z \leqslant L/2$, and on the outer boundary ($r = R_{\max}$) we prescribe the normal velocity of the corresponding potential flow and zero vorticity. Time is non-dimensionalized by the factor U_∞/R.

The equations are discretized using a vortex method, see Cottet & Koumoutsakos (2000); Ould-Sahili, Cottet & El Hamraoui (2000); Cottet & Poncet (2003); Poncet (2004); Koumoutsakos (2005), summarized as follows:

(i) The vorticity field is discretized on particles: $\boldsymbol{\omega}(\boldsymbol{x}, t) = \sum_p \boldsymbol{\omega}_p \delta(\boldsymbol{x} - \boldsymbol{x}_p(t))$.

(ii) The particles $\boldsymbol{x}_p$ are convected with the flow velocity:

$$\mathrm{d}\boldsymbol{x}_p/\mathrm{d}t = \boldsymbol{u}(\boldsymbol{x}_p, t),\ \mathrm{d}\boldsymbol{\omega}_p/\mathrm{d}t = [\nabla \boldsymbol{u}(\boldsymbol{x}_p, t)]^T\,\boldsymbol{\omega}_p.$$

A second-order Runge–Kutta scheme is used to integrate the equations of motion.

(iii) At each time step, particles are remeshed onto a cylindrical grid. On this grid the velocity field is evaluated using a second-order, FFT-based, Poisson solver and the particle strength is modified to account for vortex stretching and diffusion.

(iv) The wall boundary conditions are translated into vorticity flux that is distributed to particles in the neighbourhood of the cylinder (see for instance Poncet 2007; Koumoutsakos, Leonard & Pepin 1994; Cottet & Poncet 2003).

The Lagrangian treatment of the vorticity advection method allows the use of comparatively small computational domains and large time steps without compromising either the stability or the accuracy of the method in the presence of strong variations in the boundary conditions. In the optimization runs, the cylindrical (r, θ, z) computational domain was extended to $R_{\max} = 1 + 4\pi$, $L = \pi D$. For $Re = 300$, the resolution was set to $256 \times 128 \times 64$ grid points. For $Re = 1000$, the resolution was doubled in all directions, with a time step $\delta t = 0.0625$. In the simulations, after the control velocity is turned on, the flow is computed for 100 time units with the flow settling to its steady state after 60 time units. Simulations of 100 time units require approximately 17hours of CPU time on an Itanium 2 processor. Verification simulations were performed in a computational domain with sizes doubled in both the spanwise and radial directions.

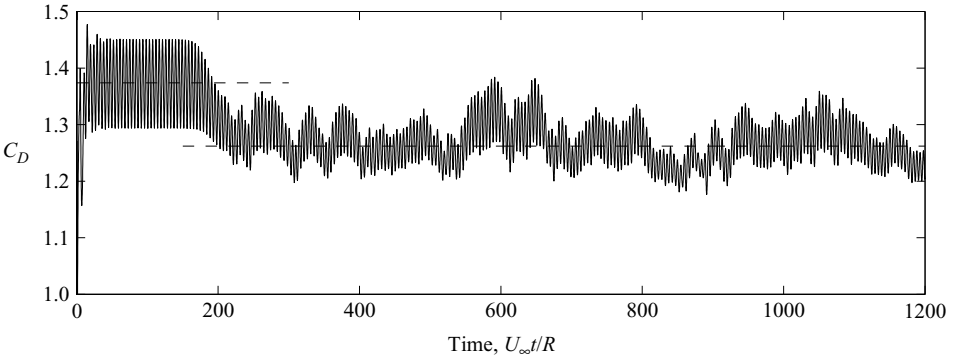

FIGURE 2. Evolution of the drag coefficient for a three-dimensional cylinder wake at $Re = 300$ (the dashed lines denote the reference values 1.374 and 1.262). The drag coefficient is initially periodic corresponding to a two-dimensional flow, until three-dimensional instabilities become the dominant feature, leading to a non-periodic signal and a lower drag value.

These simulations were used for the flow visualization and the analysis (figure 2) of the optimal profiles.

2.2. *Cylinder drag coefficient*

The cylinder drag coefficient is computed by taking the time derivative of the linear impulse of the vorticity field in the volume Ω surrounding the body:

$$C_D = -\frac{1}{U_\infty^2 R}\frac{\mathrm{d}}{\mathrm{d}t}\int_\Omega \boldsymbol{\omega}\times\boldsymbol{x}\cdot\boldsymbol{e}_x\,\mathrm{d}v \tag{2.3}$$

where $\boldsymbol{e}_x$ denotes the streamwise direction. The drag coefficient can be decomposed into contributions from the wall shear stresses (C_{DF}) and the pressure gradient (C_{DP}) on the surface of the body, which can be expressed in terms of the wall vorticity and the wall vorticity flux by:

$$C_{DF} = -\frac{\nu}{U_\infty^2 RL}\int_{\partial\Omega}\omega_z\sin\theta\,\mathrm{d}s, \qquad C_{DP} = -\frac{\nu}{U_\infty^2 RL}\int_{\partial\Omega} r\frac{\partial\omega_z}{\partial r}\sin\theta\,\mathrm{d}s.$$

The evolution of the drag coefficient follows closely the appearance of instabilities in the wake. These instabilities are associated with a reduced drag of the three-dimensional flow. The drag coefficient is initially periodic corresponding to a two-dimensional flow, until three-dimensional instabilities become the dominant feature, leading to a non-periodic signal and a lower drag value (figure 2).

The vortex method, described in the previous subsection, has been validated in Poncet (2004) in simulations of three-dimensional flows of uncontrolled cylinder wakes. The drag value of the uncontrolled flow at $Re = 300$ is 1.26, and results from averaging the flow over 1200 time units. Note that this drag coefficient is within the values of 1.32, 1.24, 1.26 reported respectively in simulations by Kim & Choi (2005); Kravchenko, Moin & Shariff (1999); Mittal & Balachandar (1995) and the 1.22 reported in experiments (Wieselsberger 1922) for the same *Re*.

3. Drag optimization

The present optimization strategy uses as a starting point the optimized azimuthal wall tangential velocity component, obtained in two-dimensional simulations using a genetic algorithm in Milano & Koumoutsakos (2002). This two-dimensional profile is uniformly extended in the spanwise direction of the cylinder and the optimization

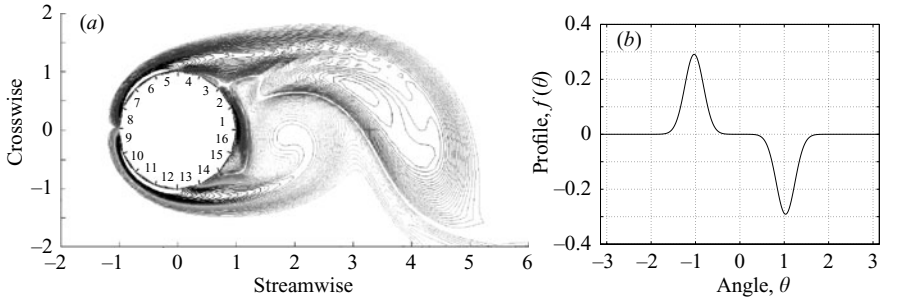

FIGURE 3. (*a*) Actuator configuration on the cylinder surface (from Milano & Koumoutsakos 2002) and (*b*) velocity profile fitting the best population obtained by the CGA.

procedure described below identifies optimal, three-dimensional, spanwise variations for enhanced drag reduction.

3.1. *Optimization of two-dimensional cylinder wakes*

The starting point of the present optimization is the two-dimensional velocity profiles obtained in Milano & Koumoutsakos (2002) using a clustering genetic algorithm (CGA). In that work the cylinder surface is divided into 16 panels, each with a steady tangential velocity that can have a value in $[-1, 1]$. The CGA operates on these 16 parameters (see Milano & Koumoutsakos 2002 for details) to identify the respective wall tangential velocities that minimize the drag coefficient. The results of that study led to a drag reduction of 50%, albeit using an order of magnitude larger energy than that reported in the present study. In addition the algorithm identified in an automated fashion, that the drag reduction was largely attributed to the motion of actuators 3–4 and 13–14 (figure 3), which contain the separation point of the uncontrolled cylinder. The velocities of the 16 actuators are fitted by the following bi-Gaussian function:

$$f(\theta) = \alpha \sum_{j=1,2} \frac{(-1)^j}{\sigma\sqrt{2\pi}} \exp\left(\frac{-(x+(-1)^j m)^2}{2\sigma^2}\right) \tag{3.1}$$

with $\alpha = 0.3342$, $m = 1.03$ and $\sigma = 0.21$. The arrangement of the belt actuators and the resulting fitted function are shown in figure 3.

3.2. *Optimization of spanwise distributed controllers*

The three-dimensional control velocity profiles of the present optimization study are spanwise modulations of the two-dimensional profile given by (3.1). The velocity profile is parameterized in terms of harmonics of the cylinder span:

$$U_\theta(\theta, z) = U_\infty f(\theta)\left(c_0 + \sqrt{2}\sum_{k=1}^{n} a_k \sin(2\pi k z/L) + b_k \cos(2\pi k z/L)\right)\boldsymbol{e}_\theta \tag{3.2}$$

where $L = \pi D$ is the spanwise length of the cylinder and the harmonics have wavelength $\lambda_k = L/k$. We have selected $n = 4$ resulting in nine parameters for the optimization.

Our choice for the wavenumber range was motivated by Poncet (2005) who considered single-mode modulations of the wall tangential velocity, and found that, at $Re = 300$, three-dimensional modulations are efficient for wavelengths up to 4. Moreover, $k = 3$ corresponds to a modulation at the closest frequency to the natural mode B instability, but it does not lead to reduced drag (except for high energy

		Mode coefficients c_0 or $(a_k^2+b_k^2)^{1/2}$					C_D	
Span	Case	$k=0$	$k=1$	$k=2$	$k=3$	$k=4$	$Re=300$	$Re=10^3$
$L=\pi D$	I	0	0	0	0	0	1.26	0.99
	II	0.316	0	0	0	0	1.143	0.93
	III	0.22	0.139	0.015	0.011	0.178	0.862	0.65

TABLE 1. Averaged drag: no control (Case I), two-dimensional control (Case II), optimal three-dimensional control (Case III).

control, Poncet 2005). On the other hand, $k=1$ reinforces the mode A instability, leading to a dramatic drop of the drag coefficient. This happens despite the flow being at a Reynolds number above 250, for which mode A is no longer visible. This range of wavenumbers is consistent with the wavelengths obtained by shape optimization in Darekar & Sherwin (2001), in which the most efficient perturbations are associated with modes $k > \pi/5.6 \simeq 0.56$.

In the present optimization all parametric studies are performed at a constant energy level. The non-dimensional kinetic energy involved in the control is determined as (Poncet *et al.* 2005):

$$E_c^* = \frac{1}{4\pi}\left(c_0^2 + \sum_k |a_k|^2 + |b_k|^2\right) \int_{-\pi}^{\pi} f(\theta)^2 \,\mathrm{d}\theta.$$

The energy level of the present control strategy was adjusted to match the levels reported in Kim & Choi (2005). The tangential profile of that blowing/suction used in that work is not available and we assume that it had an energy content equivalent to our function f. For a maximum blowing of 0.2 this gives an energy value of 0.1. We thus set

$$c_0^2 + \sum_k |a_k|^2 + |b_k|^2 = 0.1.$$

The present optimization algorithm proceeds as follows: For each pair of wavenumbers we perform 100 function evaluations on their respective plane. The energy level E_c^* is kept constant by adjusting accordingly the value of the constant mode amplitude c_0. We examine all possible pairs of wavenumbers and identify for each plane the point yielding the smallest drag coefficient. We then use these minima as starting points for a local search based on the concept of design of experiments (Box & Wilson 1951). A finite difference stencil is allocated around each point in all parametric directions and a local gradient descent algorithm is performed. The algorithm is found to converge after 4 to 5 iterations.

This optimization process for the flow past a circular cylinder at $Re=300$, results in a drag coefficient of $C_D=0.862$, corresponding to a drag reduction of about 33% (see table 1). This drag reduction is four times larger than that achieved by the corresponding two-dimensional configuration. The present results compare well with the 23% drag reduction reported in Kim & Choi (2005) for a maximum blowing/suction ranging between 0.1 and 0.2. In the present optimal configuration, the maximum tangential velocity was 0.09 for case II and 0.179 for case III, with a mean velocity of 0.074. As we optimize for a given energy level, it is not possible to match a prescribed maximum velocity. Note that in the present case the drag reduction level scales with the energy input of the control, in contrast with the observation in Kim & Choi (2005) that increasing the blowing/suction beyond 0.1 does not lead to further drag reduction.

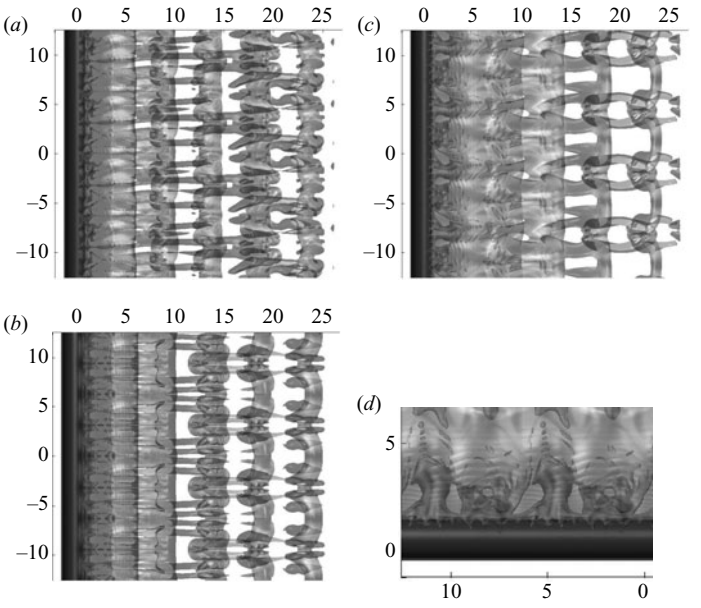

FIGURE 4. Top views of isovorticity surfaces $\|\boldsymbol{\omega}\|R/U_\infty = 0.3$, doubled by periodicity in the spanwise direction, for (*a*) the uncontrolled (case I), (*b*) two-dimensional control (case II) and (*c*, *d*) three-dimensional control (case III) for $Re = 300$, (*d*) being an enlargement of (*c*).

4. Discussion

The results of the simulations for the uncontrolled wake (case I), the wake with two-dimensional control (case II) and the wake with optimal three-dimensional control parameters (case III) are listed in table 1. For $Re = 1000$ we used the optimal parameters identified for $Re = 300$ and no further optimization was performed.

The drag reduction observed in the three-dimensional controlled flow is analysed in terms of instantaneous vorticity isosurfaces for uncontrolled and controlled wakes (figure 4). The effect of the two-dimensional control is to weaken the structures of streamwise vorticity while the optimal three-dimensional control leads to the introduction of streamwise vorticity in the wake that further weakens the strength of the primary spanwise vortices. Furthermore, in the three-dimensional control, the von Kármán streets are attached for longer to the cylinder surface thus delaying their shedding in the wake. This delayed shedding is visible in the absence of oscillations in the drag evolution for case III on figure 5. Zooming into the vorticity isosurface for case III (figure 4) we observe that strong braids of streamwise vorticity act to attach the primary vortices to the surface of the cylinder. The normal vorticity on the cylinder is correlated with spanwise variations of the slip velocity for short wavelengths. This result further justifies the choice for harmonic, rather than subharmonic control parameters, that further enhance the natural cylinder wake instabilities.

We explored the validity of this mechanism for higher Reynolds number flows by performing a DNS at $Re = 1000$. We observe that the control parameters identified for $Re = 300$ lead also to drag reduction for this higher Reynolds number. This drag reduction is much more significant than that obtained by two-dimensional control (see figure 5). On figure 6 we present contours of cross-section for the vorticity magnitude averaged in the spanwise direction and the instantaneous vorticity isosurfaces. Both two- and three-dimensional control clearly result in a strong reduction of the strength of the vortices in the wake. The three-dimensional control, although it tends to

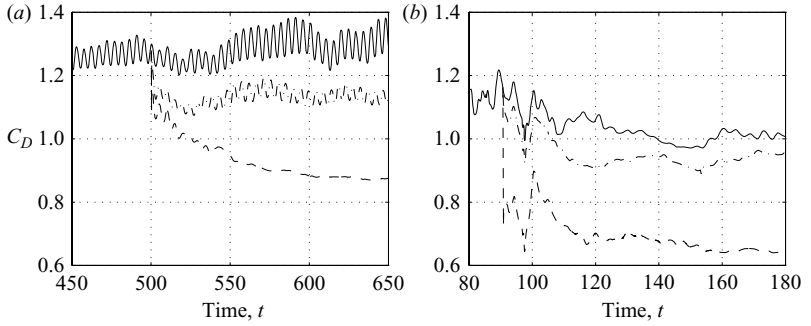

FIGURE 5. Drag time history for: uncontrolled flow (—, case I), two-dimensional control (— · —, case II), and optimal three-dimensional control (— —, case III). (*a*) $Re = 300$, (*b*) $Re = 1000$.

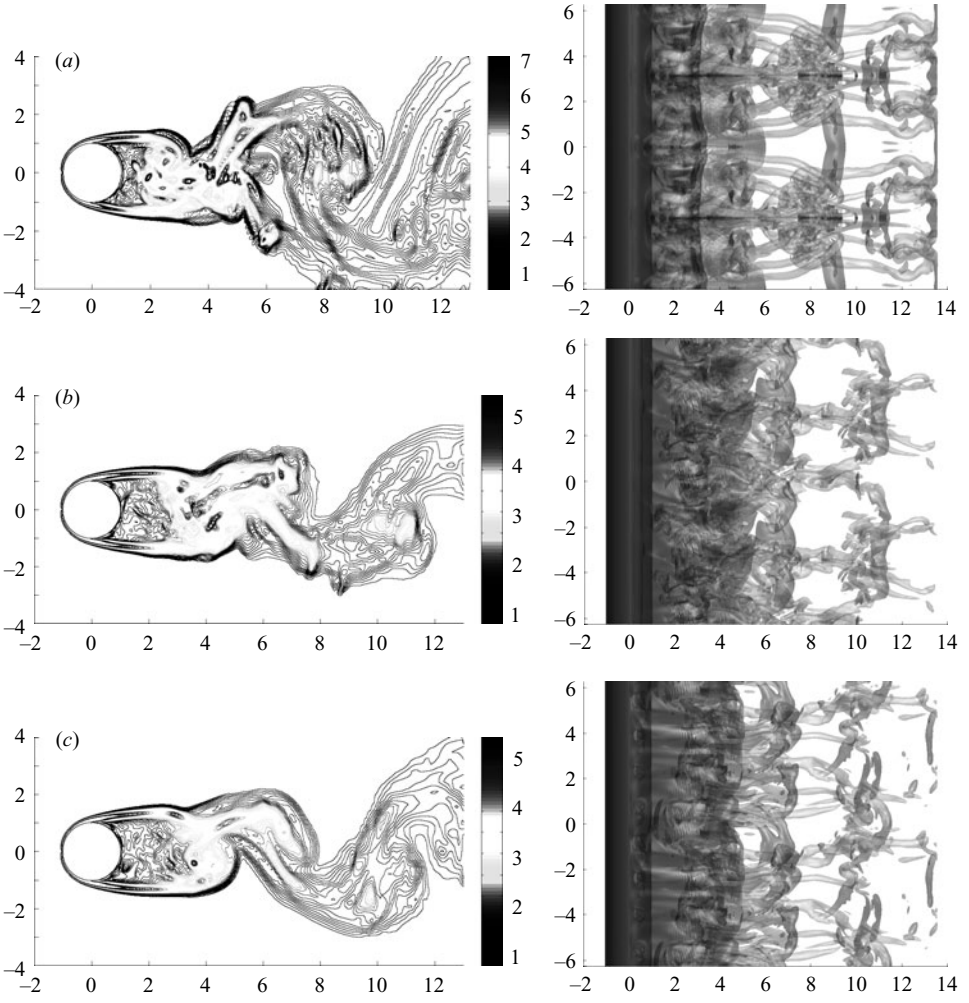

FIGURE 6. Surfaces of isovorticity $\|\boldsymbol{\omega}\| R/U_\infty = 2.4$ (right pictures) and contours of spanwise quadratic averaged vorticity (left pictures) at $Re = 1000$: (*a*) without control, (*b*) with optimal two-dimensional control, and (*c*) with the parameters of case III.

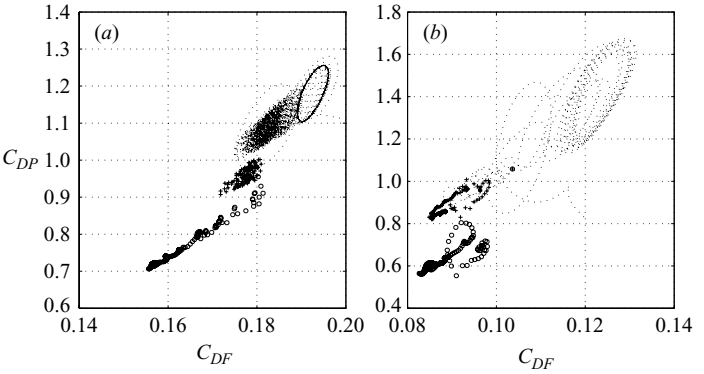

FIGURE 7. Drag coefficient pressure part C_{DP} vs. friction part C_{DF} for (*a*) $Re = 300$ and (*b*) $Re = 1000$, for uncontrolled flow (- -), two-dimensional control (+) and three-dimensional control (○).

reinforce three-dimensional instabilities, results in a smoother organization of the near wake, with strong streamwise vortex braids that are attached to the body. An inspection of the phase diagram of the friction and pressure drag (figure 7), shows that for $Re = 300$, two- and three-dimensional control lead to a systematic drop of pressure drag and to an asymptotic state for which both friction and pressure are decreased. For $Re = 1000$, the two-dimensional control does not change these quantities significantly, while the three-dimensional control acts mainly on the pressure drag.

As shown in table 1 the optimal configuration, modes 1 and 4, have coefficients that are an order of magnitude larger than those for modes 2 and 3. Since these modes are close to natural instability modes A and B (respectively of wavelength $\lambda_1/D \simeq 4$ and $\lambda_4/D \simeq 1$) and as mode A is associated with a natural drag reduction at low Reynolds numbers, we performed complementary simulations at $Re = 300$ with a cylinder span of $L = 4D$, thus matching the wavelengths of modes A and B. Using the coefficients of case I, which are probably not optimal for this span, we obtained a drag coefficient of 0.90. We next performed a simulation keeping the same coefficient values for $k = 0$, $k = 1$ and $k = 4$ and turning off modes 2 and 3. We obtained a similar drag value of 0.88. These results confirm the importance of exciting modes A and B for drag reduction. The present optimization process identified in an automated fashion this physical property of the system and allocated the proper energy distribution between these modes and the two-dimensional optimal profile to achieve maximal drag reduction.

5. Conclusions

We have demonstrated that, for a prescribed energy level, an appropriate spanwise distribution of tangential velocities can lead to significant drag reduction. The optimal control parameters have been systematically identified for a low Reynolds number flow, and shown to be also effective at moderate Reynolds numbers. The driving mechanism is the generation of strong streamwise vortex braids that delay the shedding and weaken the spanwise vorticity in the wake. The resulting optimal parameters indicate that the three-dimensional disturbances, corresponding to modes A and B of three-dimensional wake instabilities, are largely responsible for this drag reduction.

We acknowledge many discussions with Professor Michele Milano (Arizona State University) as well as several helpful suggestions from the reviewers. The second

author was supported by the French Ministry of Education through ACI grant MD-412002 which also partially provided the computational resources used in this project.

REFERENCES

Barkley, D. & Henderson, R. D. 1996 Three-dimensional Floquet stability analysis of the wake of a circular cylinder. *J. Fluid Mech.* **322**, 215–241.

Box, G. E. P. & Wilson, K. B. 1951 On the experimental attainment of optimum conditions. *J. R. Statist Soc.* **13** B, 1–38.

Choi, H., Jeon, W.-P. & Kim, J. 2008 Control of flow over a bluff body. *Annu. Rev. Fluid Mech.* **40**, 113–139.

Cottet, G.-H. & Koumoutsakos, P. D. 2000 *Vortex Methods, Theory and Practice*. Cambridge University Press.

Cottet, G.-H. & Poncet, P. 2003 Advances in Direct Numerical Simulations of three-dimensional wall-bounded flows by Vortex In Cell methods. *J. Comput. Phys* **193**, 136–158.

Cottet, G.-H. & Poncet, P. 2004 New results in the simulation and control of three-dimensional cylinder wakes. *Computers. Fluids* **33**, 697–713.

Darekar, R. M. & Sherwin, S. J. 2001 Flow past a square-section cylinder with a wavy stagnation face. *J. Fluid Mech.* **426**, 263–295.

Dennis, S. C. R., Nguyen, P. & Kocabiyik, S. 2000 The flow induced by a rotationally oscillating and translating circular cylinder. *J. Fluid Mech.* **385**, 255–286.

Dobre, A., Hangan, H. & Vickery, B. J. 2006 Wake control based on spanwise sinusoidal perturbations. *AIAA J.* **44**, 485–492.

Kim, J. & Choi, H. 2005 Distributed forcing of flow over a circular cylinder. *Phys. Fluids* **17**, 033103.

Koumoutsakos, P. 2005 Multiscale flow simulations using particles. *Annu. Rev. Fluid Mech.* **37**, 457–487.

Koumoutsakos, P., Leonard, A. & Pepin, F. 1994 Boundary conditions for viscous vortex methods. *J. Comput. Phys.* **113**, 52.

Kravchenko, A. G., Moin, P. & Shariff, K. 1999 B-spline method and zonal grids for simulations of complex turbulent flows. *J. Comput. Phys.* **151**, 757–789.

Lee, S. J., Lim, H. C., Han, M. & Lee, S. S. 2005 Flow control of circular cylinder with a V-grooved micro-riblet film. *Fluid Dyn. Res.* **37**, 246–266.

Lim, H. C. & Lee, S. J. 2004 Flow control of a circular cylinder with O-rings. *Fluid Dyn. Res.* **35**, 107–122.

Luo, S. C. & Xia, H. M. 2005 Parallel vortex shedding at $Re = O(10^4)$ – a transverse control cylinder technique approach. *J. Fluid Mech.* **541**, 134–165.

Milano, M. & Koumoutsakos, P. 2002 A clustering genetic algorithm for cylinder drag optimization. *J. Comput. Phys.* **175**, 79–107.

Mittal, R. & Balachandar, S. 1995 Effect of three-dimensionality on the lift and drag of nominally two-dimensional cylinders. *Phys. Fluids* **7**, 1841.

Ould-Sahili, M. L., Cottet, G.-H. & El Hamraoui, M. 2000 Blending finite-differencies and vortex methods for incompressible flow computations. *SIAM J. Sci. Comput.* **22**, 1655–1674.

Poncet, P. 2004 Topological aspects of the three-dimensional wake behind rotary oscillating circular cylinder. *J. Fluid Mech.* **517**, 27–53.

Poncet, P. 2005 Bimodal optimization of three-dimensional wakes. *Proc. 6th DLES Conference*, pp. 449–458.

Poncet, P. 2007 Analysis of direct three-dimensional parabolic panel methods. *SIAM J. Numer. Anal.* **45**, 2259–2297.

Poncet, P., Cottet, G.-H. & Koumoutsakos, P. 2005 Control of three-dimensional wakes using evolution strategies. *C. R. Mecanique* **333**, 65–77.

Poncet, P. & Koumoutsakos, P. 2005 Optimization of vortex shedding in 3D wakes using belt actuators. *Intl J. Offshore Polar Engng* **15**, 7–14.

Tokumaru, P. & Dimotakis, P. 1991 Rotary oscillation of a cylinder wake. J. Fluid Mech. **224**, 77–90.

Wieselsberger, C. 1922 New data on the laws of fluid resistance. *Report NACA-TN*-84.

Williamson, C. H. K. 1996 Vortex dynamics in the cylinder wake. *Annu. Rev. Fluid Mech.* **28**, 477–526.